

A Test for the Nature of the Type Ia Supernova Explosion Mechanism

Philip A. Pinto¹

*Steward Observatory
University of Arizona
Tucson, AZ 85721 USA*

ppinto@as.arizona.edu

Ronald G. Eastman²

*Lawrence Livermore National Laboratory
Livermore, CA 94550 USA*

reastman@llnl.gov

and

Tamara Rogers¹

*Department of Astronomy and Astrophysics
University of California Santa Cruz,
Santa Cruz CA 95064 USA*

tami@ucolick.org

ABSTRACT

Currently popular models for Type Ia supernovæ (SNe Ia) fall into two general classes. The first comprises explosions of nearly pure carbon/oxygen (C/O) white dwarfs at the Chandrasekhar limit which ignite near their centers. The second consists of lower-mass C/O cores which are ignited by the detonation of an accreted surface helium layer. Explosions of the latter type produce copious Fe, Co and Ni K α emission from ^{56}Ni and ^{56}Co decay in the detonated surface layers, emission which is much weaker from Chandrasekhar-mass models. The presence of this emission provides a simple and unambiguous discriminant between these two models for SNe Ia. Both mechanisms may produce $0.1 - 0.6M_{\odot}$ of ^{56}Ni , making them bright γ -ray line emitters. The time to maximum brightness of ^{56}Ni decay lines is distinctly shorter in the $M < M_{ch}$ class of model (~ 15 days) than in the M_{ch} model (~ 30 days), making γ -ray line evolution

¹Lawrence Livermore National Laboratory, Livermore CA 94550 USA

²Department of Astronomy and Astrophysics, University of California, Santa Cruz, Santa Cruz CA 95064 USA

another direct test of the explosion mechanism. It should just be possible to detect K-shell emission from a sub- M_{ch} explosion from SNe Ia as far away as the Virgo cluster with the XMM Observatory. A 1 to 2 (meter)² X-ray telescope such as the proposed Con-X Observatory could observe $K\alpha$ emission from $M < M_{\text{ch}}$ SNe Ia in the Virgo cluster, providing not just a detection, but high-accuracy flux and kinematic information.

Subject headings: stars:X-rays – gamma rays:general – radiation mechanisms – stars:supernovae

1. Introduction

The luminosity of Type Ia supernovae (SNe Ia), the brightest stellar explosions, arises in current successful models not from the energy of the explosion itself but from the radioactive decay of ^{56}Ni . Following Arnett (1980), in all current models these explosions are the thermonuclear incineration of a white dwarf. The very compact nature of this progenitor ensures that the explosion energy is efficiently converted to kinetic energy of expansion (*c.f.* Pinto & Eastman (2000b) for a discussion and further references). If a significant luminosity is to be developed, energy must be injected at later times when the column depth of the ejecta has declined significantly and radiation can escape.

It is by now widely recognized that this later deposition of energy results from the radioactive decay of ^{56}Ni . This isotope is a by-product of burning to nuclear statistical equilibrium (NSE), the process which is responsible for liberating much of the energy which disrupts the star. While γ -rays from ^{56}Ni decay have yet to be observed from SNe Ia, the evidence from the temporal behavior of the light curve (Colgate & McKee 1969; Clayton et al. 1969) and from optical and infrared spectra (Axelrod 1980; Weaver et al. 1980; Kuchner et al. 1994) is very strong. It is further strengthened by the success of the radioactive decay model in explaining the light curve of SN 1987A (Xu 1989; Pinto & Woosley 1988b,a; Pinto et al. 1988), from which γ -rays *were* directly observed (Gehrels et al. (1988) and references therein). Just as the X- and γ -ray emission from SN1987A yielded new and important information about the dynamics of its explosion, so too observations of SNe Ia at these energies hold the promise of significant advances.

Despite 30 years of observation and theoretical study, progress towards understanding the detailed set of events and the physics leading to SNe Ia explosions remains elusive. In particular, the last decade has seen intense observational efforts in the optical and near IR and matching theoretical activity. Though we have learned a great deal about SNe Ia, it must still be said that incorporating current data into a tight theoretical picture remains an enterprise fraught with difficulty. SNe Ia explosion models are frustrated by uncertainties about thermonuclear flame physics and progenitor evolution, while the interpretation of optical data is hindered by uncertainties in the non-LTE atomic physics of nearly-neutral silicon-, and especially, iron-group ions.

If there exists a “standard model” for SNe Ia, the current definition would be a C-O WD in a close binary system which is pushed by accretion very near the Chandrasekhar mass limit, 1.38

M_{\odot} . As the central density of the dwarf rises above 10^9 g cm^{-3} , carbon ignites near the center, leading to an outward-propagating thermonuclear flame. This flame is Rayleigh-Taylor unstable and very quickly becomes turbulent, leading to a marked acceleration in its progress, as necessary to achieve an energetic explosion (*c.f.* Woosley & Weaver (1986)). This turbulence also makes direct numerical simulation intractable (Niemeyer & Woosley (1997); Khokhlov et al. (1997), and references therein); current models are thus hampered by a lack of predictive power.

A possible alternative to the standard model, or perhaps an *addition* to it, is a C-O WD in the mass range $0.6M_{\odot} - 0.9M_{\odot}$, bound to a helium main sequence companion burning helium at its center. Accretion in such systems was studied by Limongi & Tornambe (1991) who found that for accretion rates near $\sim 3 \times 10^{-8} M_{\odot} - \text{yr}^{-1}$, of order $0.2 M_{\odot}$ of helium could be accreted until this layer detonated near its base. As others have noted, this is very near the accretion rate estimated by Iben & Tutukov (1991) who found this rate, driven by gravitational wave radiation, to be insensitive to the mass ratio of the two components, thereby alleviating the need to fine-tune progenitor properties to result in such an explosion.

The possibility that this ignition mechanism might lead to a Type Ia supernova was first suggested by Livne (1990), and studied in 2-D by Livne & Glasner (1991). In one dimensional models, detonation in the helium layer produces an inward moving, focused compression wave which drives the central density above 10^8 g cm^{-3} and temperature above 10^9 K , causing central carbon ignition under explosive conditions. The subsequent evolution and nucleosynthesis was studied by Woosley & Weaver (1994) in 1-D, and by Livne & Arnett (1995) in 2-D. While the progress of the explosion is rather different in 2-D, both calculations produce very similar results which may indicate the robustness of this mechanism. The models possess a number of attractive properties, such as production of $0.1 - 0.9 M_{\odot}$ of ^{56}Ni , with the remainder of the original CO WD going to silicon group isotopes. As Woosley & Weaver have pointed out, such sub- M_{ch} models may be the production sites for ^{44}Ca (produced as ^{44}Ti), and ^{48}Ti (made as ^{48}Cr), neither of which are accounted for by either Type II supernovae or M_{ch} SNe Ia (Timmes et al. 1995). Even more attractive is the fact that, since burning takes place at lower densities than in M_{ch} stars, these models do not suffer from the problem of excess electron capture and the resultant over-production of rare neutron-rich species, such as ^{54}Fe , ^{58}Fe , ^{54}Cr , and ^{58}Ni which plague M_{ch} models (though accretion at extremely high rates accompanied by strong winds may be able to cure this, *c.f.* Brachwitz et al. (2000)). The amount of ^{56}Ni produced increases monotonically with the mass of the WD, implying greater maximum brightness for more massive stars. The increased mass may also mean a longer diffusion time, and the correlation of both these properties is in the right direction to explain the maximum brightness-decline rate relationship described by Phillips (1993). There is some hint of this in the bolometric light curves computed by Woosley & Weaver and by Livne & Arnett, but a more accurate comparison with observations requires multigroup transport with velocity broadened line opacities as in Pinto & Eastman (2000b).

It is not known what fraction, if any, of observed SNe Ia are due to sub- M_{ch} explosions. Iben & Tutukov (1991) estimated the rate for He symbiotic systems to explode at the rate of 1 per

century in the galaxy, which compares well with the SNe Ia rate determined by van den Bergh & Tammann (1991), Cappellaro et al. (1997), and Hamuy & Pinto (1999). In principle, it ought to be possible to distinguish M_{ch} and sub- M_{ch} explosion models from their predicted optical light curve and spectral evolution. Years of tuning M_{ch} models to achieve a match between observed and computed spectra have resulted in a defining list of properties which the successful Ia explosion must possess. “Successful” models include the Nomoto et al. (1984) Model W7 (Harkness 1991) and the Woosley & Weaver (1991) Model DD4 (Kirshner et al. 1993; Eastman 1996; Pinto 1997; Pinto & Eastman 2000b). Sub- M_{ch} models have, on the other hand, remained largely unexplored, though some sub- M_{ch} models share many of the same desirable properties as their more massive cousins. The spectra of current sub- M_{ch} models reported in the literature are too blue (Nugent et al. 1997; Höflich et al. 1996) resulting in part from the presence of iron and radioactivity in the outer layers. They also have not produced, to date, Ca at sufficiently high velocities to match a typical SNe Ia. We feel these results are far from conclusive, however. Models for sub- M_{ch} explosions have not yet undergone the same degree of tuning as their more massive cousins to bring them into better agreement with observation. Current spectrum and light curve calculations are rendered uncertain by their lack of time dependence, especially in the high velocity, low density surface layers.

Since the sub- M_{ch} models have less mass (*e.g.* 0.8 versus 1.38 M_{\odot}), they might be expected to reach maximum light in less time than a M_{ch} explosion. Estimates by Contardo & Leibundgut (1998) and Riess et al. (1999) give rise times for nearby SNe Ia in the range 19 to 23 days in B. It would be nice if radiation transport simulations of the light curve evolution were accurate enough to conclusively rule out sub- M_{ch} models (or M_{ch} models) by comparison with observations. Unfortunately, the effective opacities, and even much of the basic physics, used in most calculations performed to date remain highly uncertain. To be confident in estimates of the rise time, one requires knowledge of the UV line opacity of low-ionization nickel and cobalt – opacities accurate to a factor much smaller than the mass difference between M_{ch} and sub- M_{ch} SNe models. Errors in the opacity, which comes principally from velocity-broadened UV lines of nickel, cobalt, and iron, translate directly into errors in the rise time and peak brightness (Pinto & Eastman 2000a,b). Most SNe Ia light curve calculations (*e.g.* Höflich et al. (1993); Pinto & Eastman (2000b)) have been based solely on lines from the Kurucz list (Kurucz 1991), which likely underestimates the nickel and cobalt opacities significantly. We have compared Rosseland mean opacity values computed for a pure cobalt composition at $\rho = 10^{-12}$ g cm $^{-3}$ and $T = 20,000$ K using the Kurucz list and transition data from the OPAL opacity code (Iglesias et al. 1990, 1992) and find that the OPAL opacity value is approximately 5 times larger. Thus, in the M_{ch} calculations by Höflich et al. (1996), the model with the slowest rise time still reaches bolometric maximum light in only 15 days. In a light curve calculation by Pinto & Eastman (2000b) of a similar model, the predicted bolometric maximum light was at 15 days, even though the *B* and *V* light curves did not peak until 20 days. However, the available evidence is that the time of bolometric maximum corresponds to the time of *B* maximum. Such discrepancies are enough to raise questions about the accuracy of current calculations and to doubt claims that sub- M_{ch} models are, at present, quite ruled out on theoretical grounds.

In this paper we present a simple test of the sub- M_{ch} model which is quite insensitive to most details of either the modeling or the exact nature of the supernovæ themselves. It is based upon the fact that the surface helium detonation in most sub- M_{ch} models produces significant yields of ^{56}Ni at high velocities which are absent in the M_{ch} models. High energy photons produced by the decay of ^{56}Ni can therefore escape largely unimpeded from these surface layers, while photons released by decay in the radioactive core are strongly attenuated. A lack of observed high-energy emission at early times from SNe Ia would thus argue strongly, and probably fatally, against the sub- M_{ch} model. On the other hand, detection of early emission at high energies would argue strongly in favor of these models, as it is difficult to produce significant quantities of radioactivity in the surface layers of M_{ch} explosions. (While hydrodynamic mixing in pure C-O models might conceivably lead to significant ^{56}Ni at high velocities as well, the compositional stratification deduced from early-time spectra would be destroyed by such a process.) As we shall show, the decay of surface ^{56}Ni in sub- M_{ch} explosions produces considerable Fe, Co and Ni $K\alpha$ emission between 6 and 8 keV, at flux levels great enough to be detected from extragalactic supernovae, possibly by current and upcoming missions, and almost certainly by the proposed Con-X Observatory. They also emit ^{56}Ni decay lines which, due to the 6.1 day half-life of ^{56}Ni , peak earlier and at higher luminosities than in M_{ch} models.

Most aspects of γ -ray transport in SNe Ia (and supernovae in general) have been thoroughly explored and reported on elsewhere. The γ -ray and hard (Compton scattering) X-ray continuum evolution of typical M_{ch} explosion model was discussed by Gehrels et al. (1987), and especially by Burrows & The (1990) and Burrows et al. (1991). Clayton & The (1991) investigated γ -ray transport in M_{ch} SNe Ia models, specifically W7, and discussed the importance of bremsstrahlung emission in forming the keV X-ray continuum. Höflich et al. (1998) presented results of Monte Carlo γ -ray transport calculations for both M_{ch} and sub- M_{ch} explosion models, and pointed out differences in ^{56}Ni γ -ray line light curve evolution (see section 3). However, the present work is the first to describe the X-ray properties of sub- M_{ch} explosion models, and to propose observations which clearly discriminate between explosion models. In addition, there are significant differences between our γ -ray results for sub- M_{ch} models and those obtained by Höflich et al. (1998) which we shall describe below.

The remainder of this paper is organized as follows: in section 2 we briefly describe the methods used for our calculations. In section 3 we summarize properties of the models we have investigated – more detailed descriptions can be found in the original references – and present our results, describing and comparing the X-ray and γ -ray spectral evolution of M_{ch} and sub- M_{ch} models. In section 4 we discuss prospects for positively detecting the unique properties of a sub- M_{ch} event with current and future X- and γ -ray missions. In section 5 we describe the evolution of γ -ray line profiles and what we might learn with sufficient sensitivity. Section 6 gives a short summary of the results.

2. Computational Methods

The transport of nuclear decay γ -rays was computed using an updated version of the Monte Carlo (MC) γ -ray transport code FASTGAM (Pinto & Woosley 1987). FASTGAM includes pair production and photoelectric opacities and incorporates Compton scattering in the limit of zero electron temperature. It follows photons emitted by nuclear decay, pair annihilation, and fluorescence following K-, L-, and M-shell vacancies (induced both by photoionization and electron capture). These photons are followed until they escape from the supernova or are destroyed by absorption. FASTGAM computes the energy deposition which results from these processes, the primary electron energy spectrum produced by Compton recoil, and the emergent γ -ray spectrum.

Because the supernova ejecta are ionized, these primary electrons, with kinetic energies ranging up to ~ 1 MeV, lose energy primarily by exciting collective plasma oscillations. Other loss mechanisms include atomic ionization and excitation, and, as first noted by Clayton & The (1991), they also copiously produce bremsstrahlung X-rays. Under certain conditions which we discuss below, these X-rays dominate the continuum emission from ~ 1 to ~ 50 keV.

Because the transport equation is linear in the emissivity, the bremsstrahlung spectrum can be calculated separately from the MC code and then added linearly to the primary γ -ray spectrum calculated by FASTGAM. Therefore, following the MC calculation, the bremsstrahlung contribution was computed deterministically using a 1-D, spherical, multi-frequency comoving frame transport code (Eastman & Pinto 1993). The opacity is dominated by K- and L-shell photoionization, followed by electron scattering. The spectrum of primary Compton electrons, $S(E)$ ($\text{e}^- \text{s}^{-1} \text{erg}^{-1} \text{atom}^{-1}$) resulting from the MC calculation is used to compute the bremsstrahlung emissivity and solve for the emergent X-ray continuum flux.

The bremsstrahlung emissivity was computed using the *continuous slowing down approximation*, given by

$$\eta_\nu = \frac{h\nu}{4\pi} \int_{h\nu}^{\infty} dE S(E) \sum_Z N_Z \int_{h\nu}^E \frac{\partial \sigma_Z(E')/\partial \nu}{L(E')} dE' \quad [\text{ergs cm}^{-3} \text{s}^{-1} \text{Hz}^{-1} \text{ster}^{-1}] \quad (1)$$

where $L(E)$ is the *loss function*: the e-folding path length for the electron's energy (*c.f.* Axelrod (1980)). The partial bremsstrahlung cross section, $\partial \sigma_Z(E')/\partial \nu$, for an electron of energy E to produce a photon of frequency ν while interacting with a nucleus of charge Z , was taken from the numerical calculations of Kissel et al. (1991). The output of the deterministic transport calculation is the monochromatic photon energy density as a function of depth through the gas and the emergent X-ray flux as measured in the observer frame.

The X-ray continuum from bremsstrahlung emission is capable of producing additional K-shell vacancies. For instance, photons with energy > 7.117 keV are capable of ionizing iron. These additional vacancies contribute to the $K\alpha$ production rate, and were not included in the MC calculation. A further source of vacancies comes from direct impact ionization of the K-shell by non-thermal electrons, however The et al. (1994) have shown that the collisional ionization contribution is negli-

gible at early times. The photoionization contribution to the K-shell vacancy rate was included as follows: the monochromatic photon energy density obtained from the deterministic transport solution was used to compute the additional K-shell photoionization rate. These were combined with fluorescence yields (Kaastra & Mewe 1993) for $K\alpha$ and $K\beta$ emission following a K-shell vacancy to obtain the line emissivities. These were then used to perform another deterministic transport calculation (the opacity is the same as for the bremsstrahlung calculation), giving the emergent flux, in the observer frame, of K-shell lines produced from photoionization by bremsstrahlung X-rays; it is at most a few percent contribution.

To summarize, the composite spectrum is computed in three steps; 1) the transport of decay γ -rays is calculated using a Monte-Carlo code which gives the emergent spectrum of unscattered and down-scattered γ -rays, the K-shell line flux, and the spectrum of primary, Compton scattered electrons. 2) We use the *continuous slowing down* approximation to compute the bremsstrahlung emissivity, which is plugged into a deterministic transport code to obtain the monochromatic X-ray photon energy density and the emergent bremsstrahlung x-ray spectrum. 3) Additional K-shell line production produced when bremsstrahlung X-rays photoionize $1s$ electrons, is accounted for in a final step. All that is needed for this is the photoionization rate, which is computed using the monochromatic X-ray photon energy density obtained in step 2. The emergent spectra obtained from these three steps are added together to produce the final, composite spectrum.

The inner-shell photoionization rate due to X-rays is small compared with the rate from primary γ -rays. The loss function is determined primarily by the ionization state of the gas, and this is determined in turn by the balance of valance-shell photoionization by UV photons and radiative recombination. Thus, a fully self-consistent calculation would require a complete solution of the radiation transport and statistical equilibrium at all energies from the γ -ray to the infrared. For a gas with free (thermal) electron density $n_e \gtrsim n_{ion}$, however, the loss function is insensitive to ionization, a condition which the supernova ejecta satisfy throughout their evolution. Our three-step procedure, MC γ -ray transport, bremsstrahlung from primary and secondary electrons, and additional K-shell lines from X-ray photoionization, can thus be expected to closely approximate a full, self-consistent solution.

The emergent spectrum computed by FASTGAM consists primarily of velocity broadened γ -ray decay lines superimposed upon a smooth, Compton scattering continuum. Sampling the emergent intensity with enough energy resolution to produce accurate line fluxes requires a large expenditure of computing time. As the opacity for γ -ray lines is absorptive (Compton scattering *into* the line profile, while included in the MC treatment, is negligible), a simpler procedure is to compute individual line fluxes directly using a deterministic transport algorithm. The procedure for this is straightforward and was described in Pinto & Woosley (1988a) and Eastman et al. (1994) (we note however that that in the present work we have used $\theta_{sc} = 56^\circ$ for the mean scattering angle). This deterministic approach to computing γ -ray line transport is approximate, less accurate than MC for computing energy deposition, and does not give the Compton continuum; it does do a fine job, however, at correctly predicting the ν -integrated emergent line fluxes. This is shown in Figure 1,

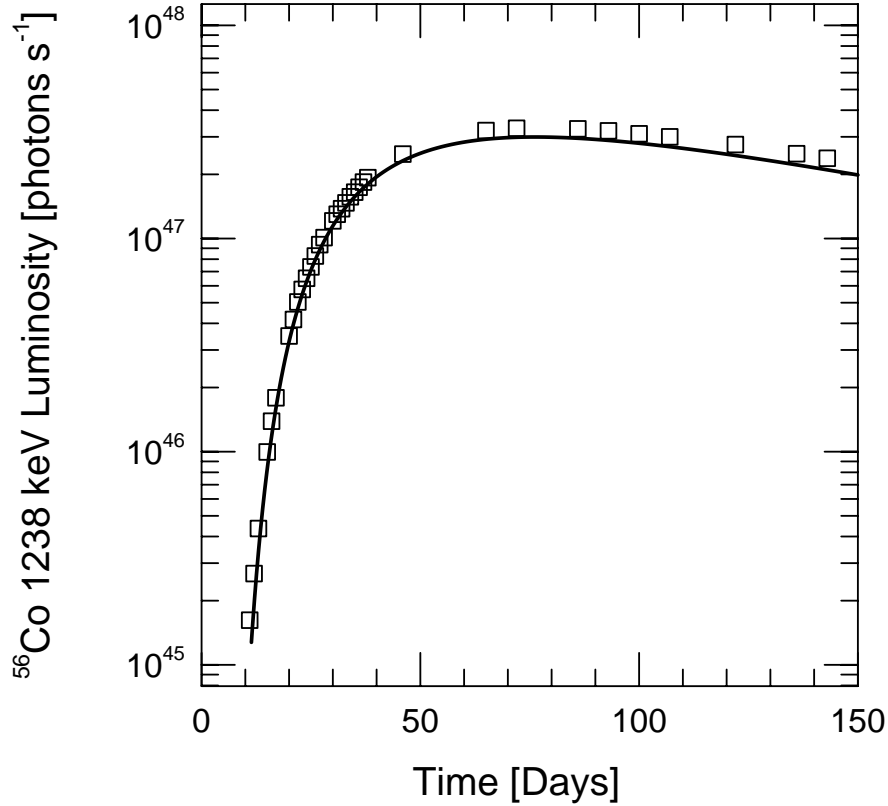


Fig. 1.— Comparison of the ^{56}Co 1238 keV line light curve for Model W7, as computed with the Monte Carlo code FASTGAM (squares), to that computed using the deterministic transport method described in section 2.

which compares the ^{56}Co 1238 keV line light curve for Model W7 computed deterministically and with FASTGAM.

3. Results

The models investigated in this paper consist of two M_{ch} mass models and three sub- M_{ch} models. The properties of these models are summarized in Table 1.

The M_{ch} models include Model W7 by Nomoto et al. (1984) and Model DD4 by Woosley & Weaver (1991). The X-ray and γ -ray spectral evolution of Model W7 was studied both by Burrows & The (1990) and by Clayton & The (1991). Model DD4 is similar in many respects to Model W7, in terms of mass, energy and total mass of ^{56}Ni produced, although in DD4 the flame speed, which in both models was an adjusted parameter, was allowed to exceed the sound speed and become a detonation, whereas in Model W7 the flame remained subsonic. The result is that in W7 only $0.29 M_{\odot}$ of “silicon group” nuclei (by which we mean ^{24}Mg through ^{40}Ca) was produced, whereas in

DD4 there is $0.49 M_{\odot}$. Despite this, both models have been shown to give reasonable agreement to spectral observations of maximum light supernovae (Harkness 1991; Kirshner et al. 1993). It is not clear whether this indicates a lack a sensitivity of such calculations to distinguish large abundance differences, or a large inherent variation in the objects themselves.

The sub- M_{ch} models investigated include Model 2 by Woosley & Weaver (1994), and Models M1 and M8 from Livne & Arnett (1995). Whereas Model 2 was a 1-D calculation, Models M1 and M8 were 2-D, and have been mapped into a 1-D, angle averaged structure (courtesy of Professor Arnett). In terms of the initial C-O white dwarf mass, the total mass, the amount of accreted helium, the total amount of ^{56}Ni produced and the final explosion energy, these three models span a large range of properties.

Figure 2 shows the composition, density and velocity structure of Model DD4, which may be compared to that of Model 2, shown in Figure 3. The biggest difference between the two classes of models, for present purposes, is the large mass fraction of ^{56}Ni on the surface of the sub- M_{ch} models.

Figure 4 compares the 20 day spectra of Models 2 and DD4. One consequence of the surface ^{56}Ni in the sub- M_{ch} models is the strong $K\alpha$ line at 7 keV. This feature is completely absent from M_{ch} models. In Model 2 (and the other sub- M_{ch} models), K-shell line emission is superimposed upon a bright bremsstrahlung continuum, dominating the spectrum near 7 keV. At 20 days this feature is a combination of contributions from Ni (10 percent) Co (73 percent) and Fe (16 percent), reflecting the relative abundances of these ions at the time. The energies and fluorescence yields for the 12 contributing lines, taken from Kaastra & Mewe (1993), are summarized in Table 2. For all three elements, roughly 30 percent of the emission is due to the $K\alpha_2$ transition, 59 percent to $K\alpha_1$, 4 percent to $K\beta_3$ and the remaining 7 percent to $K\beta_1$. The effect of the continuum edges of the Fe, Co and Ni K-shell photoionization crosssections near $E \gtrsim 7$ keV is clearly evident in the Model 2 spectrum. The jump is strong in Model 2 because the the outer material is rich in Fe peak elements. No such jump is present in the spectrum of Model DD4, because the Fe abundance is much lower in the outer part of the ejecta, dominated as it is by silicon group elements and

Table 1: Properties of Explosion Models

name	M_{tot}	M_{CO}	M_{He}	E_{51}	$M(^{56}\text{Ni})$	$M(^{56}\text{Ni})$ (surface)	$M(\text{Si group})$	ref
Model 2	0.90	0.70	0.20	0.90	0.43	0.09	0.29	a
M1	0.70	0.55	0.15	0.69	0.14	0.03	0.26	b
M8	1.10	0.90	0.20	0.25	0.71	0.17	0.25	b
W7	1.38	1.38	0	1.2	0.63	0.0	0.29	c
DD4	1.39	1.39	0	1.2	0.63	0.0	0.49	d

Table 1: Properties of explosions models considered in this paper. For a more detailed description, refer to the original references: a) Woosley & Weaver 1994; b) Livne & Arnett 1995; Nomoto, Thielemann & Yokoi 1984; d) Woosley & Weaver 1991.

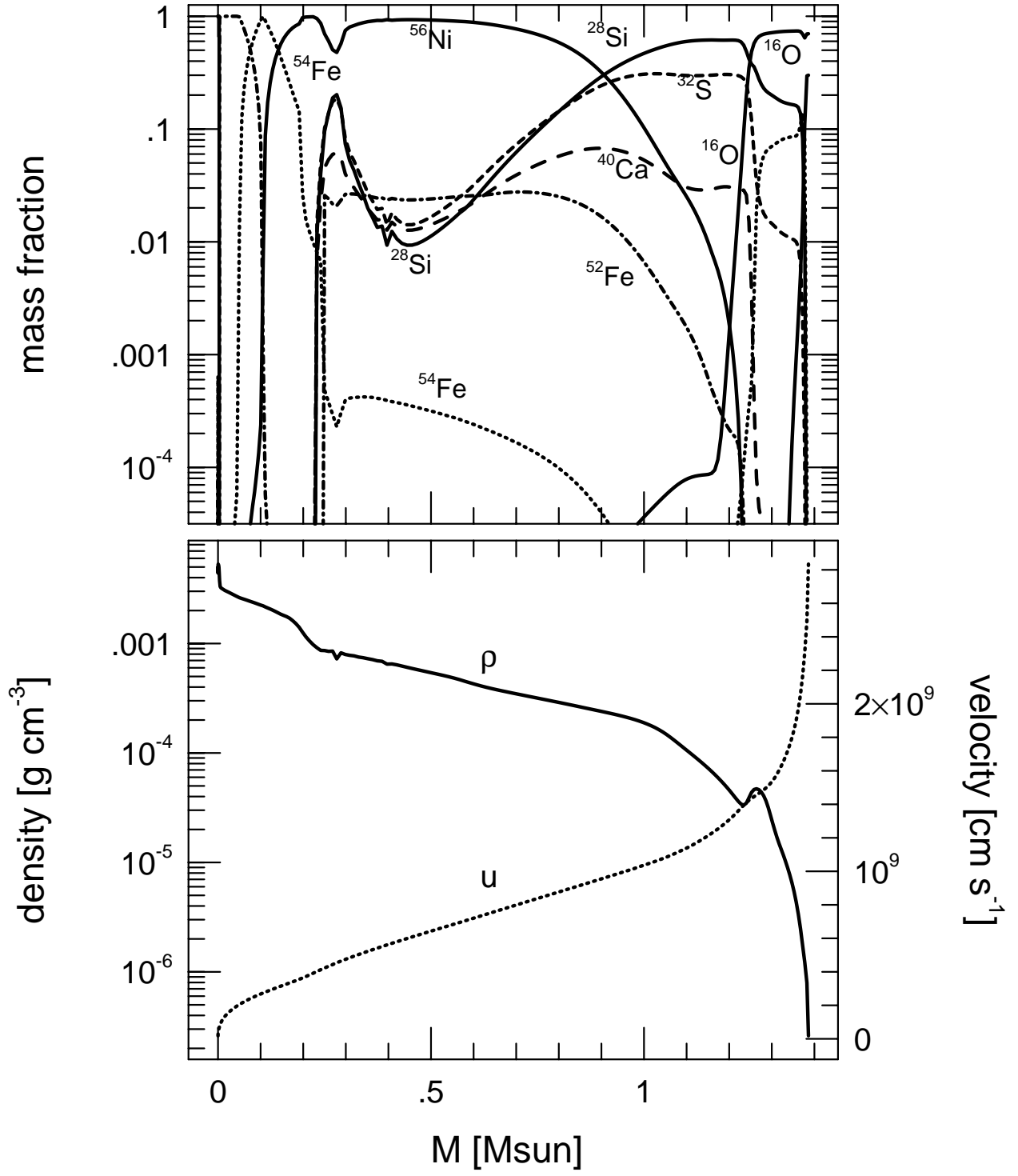


Fig. 2.— Composition, density and velocity structure of the M_{ch} delayed detonation Model DD4 (Woosley & Weaver 1991), at 1000 seconds after explosion.

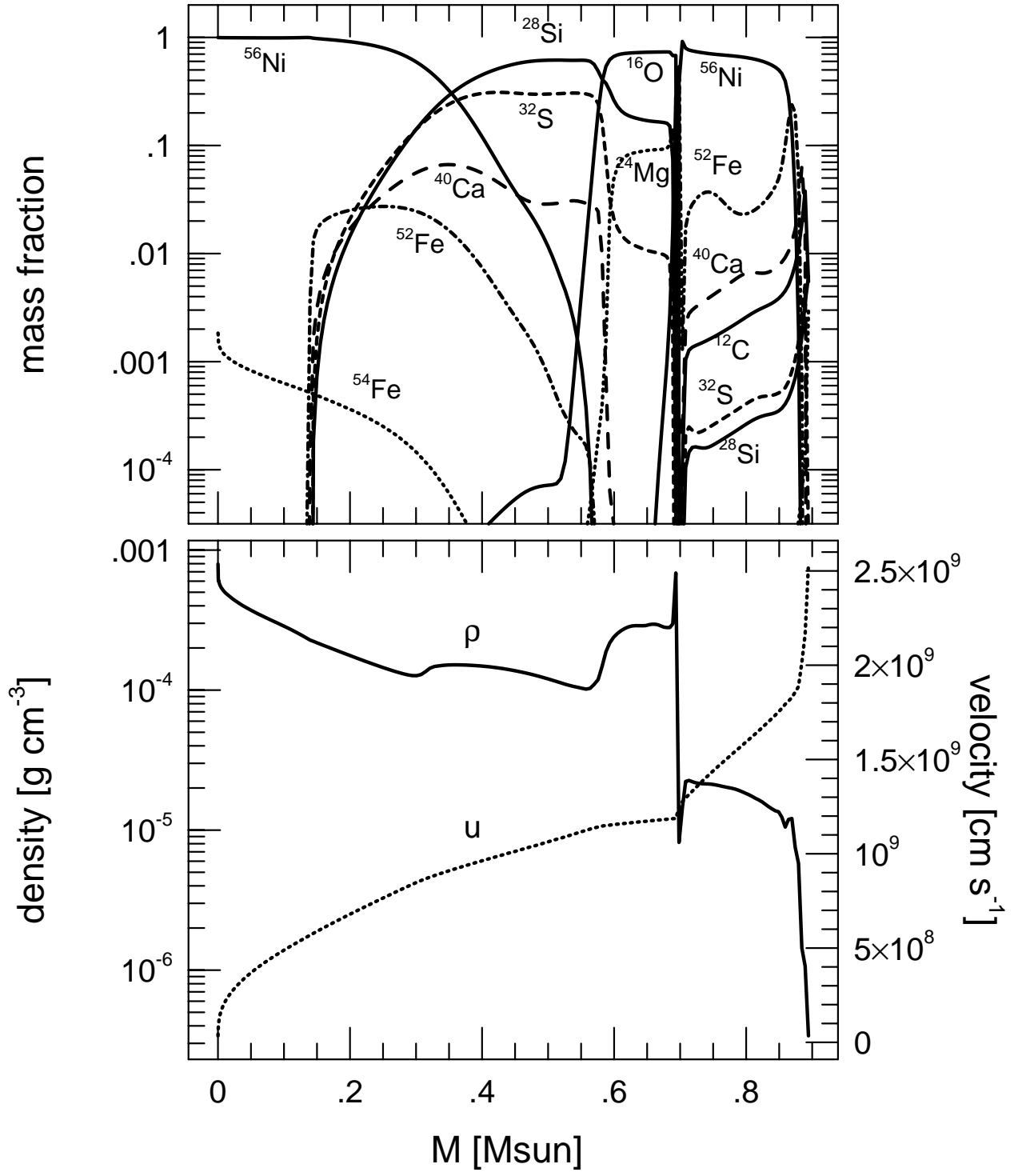


Fig. 3.— Composition, density and velocity structure of the sub- M_{ch} , edge-lit helium detonation Model 2 (Woosley & Weaver 1994), at 1000 seconds after explosion.

unburned carbon and oxygen.

Although both Models DD4 and W7 have $0.63 M_{\odot}$ of ^{56}Ni , and therefore produce a large number of $K\alpha$ photons, the optical depth at 7 keV remains large enough to absorb the X-ray emission from the ^{56}Ni core until several hundred days after explosion. This is shown by Figures 5 and 6, which compare the optical depth at 7 keV to the ^{56}Ni mass fraction in Models 2 and DD4, respectively, at 100 days. As the opacity is not affected by ionization (for low mean ionization), the optical depth at other times can be obtained by scaling as $\tau \propto t^{-2}$. Most of the optical depth at 7 keV is due to L-shell photoionization. Only emission from material at $\tau \lesssim 1$ is able to escape the surface. Consequently, the emergent K-shell line emission is due entirely to the presence of ^{56}Ni on the surface.

Spectra from Model 2 at various times during the first 160 days are shown in Figure 7. These should be compared with the spectra of Model DD4 at the same times after explosion from Figure 8. At times $t \lesssim 100$ days, the $E \gtrsim 50$ keV spectrum in both cases is dominated by narrow (see below) γ -ray decay lines superimposed on a Compton scattering continuum produced from down-scattered γ -rays. As the column density declines with time, the Compton optical depth decreases below unity and the Compton continuum eventually disappears. An excellent discussion of the evolution of the Compton continuum is given by Xu (1989) and Xu et al. (1991). The smooth continuum at $E \lesssim 50$ keV is due to bremsstrahlung emission.

In Figure 7, the strong feature at 14.4 keV which is visible in the 100 day spectra and afterwards is a nuclear decay line of ^{57}Co . The abundance of ^{57}Co was assumed to be given by the solar $^{57}\text{Fe}/^{56}\text{Fe}$ ratio (0.027), times the ^{56}Ni mass fraction in the model. As with the K-shell lines, this line will only be visible in a sub- M_{ch} explosion – the optical depth to core ^{57}Co is too great for any appreciable escape to occur.

The time evolution of the integrated K-shell line luminosity for all models is shown in Figure 9. The effect of the surface ^{56}Ni is dramatic. Again, because of the large optical depth to core ^{56}Ni , only $K\alpha$ emission produced on the surface is able to escape, with the result that even Model M1, which has only 22 percent as much ^{56}Ni as Model W7, is nearly 100 times brighter in the $K\alpha$ line than W7.

The bremsstrahlung continuum time evolution behaves somewhat differently than that of the K-shell lines – at least in the M_{ch} models. Figure 10 compares the time evolution of the integrated 5 to 8 keV continuum luminosity, excluding contributions from K-shell line emission, for each of the models. In the M_{ch} models, the emergent X-ray flux must all come from the core. The continuum emission which reaches the surface is produced at somewhat higher energy, where the K-shell bound-free opacity is lower. However, the Compton optical depth is not negligible, and photons are Doppler shifted by the bulk expansion of the gas as they diffuse out. The amount by which a photon’s energy is reduced in diffusing to the surface can be estimated as

$$\frac{\Delta E}{E} \sim \frac{l}{ct} \sim \frac{3R^2 \rho \kappa}{ct} \quad (2)$$

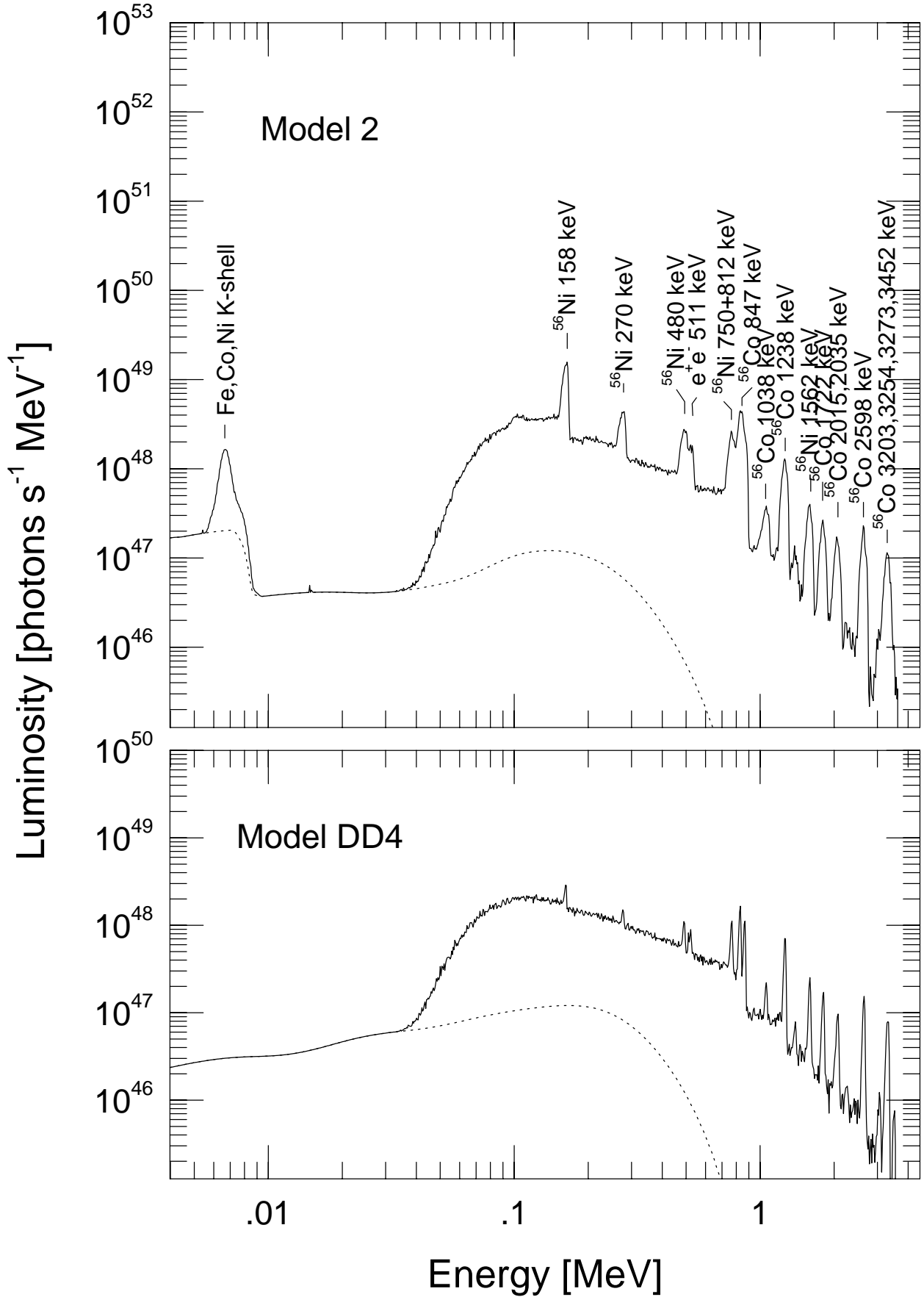


Fig. 4.— Comparison of the 20 day spectra of Model 2 and DD4. The dotted line shows the

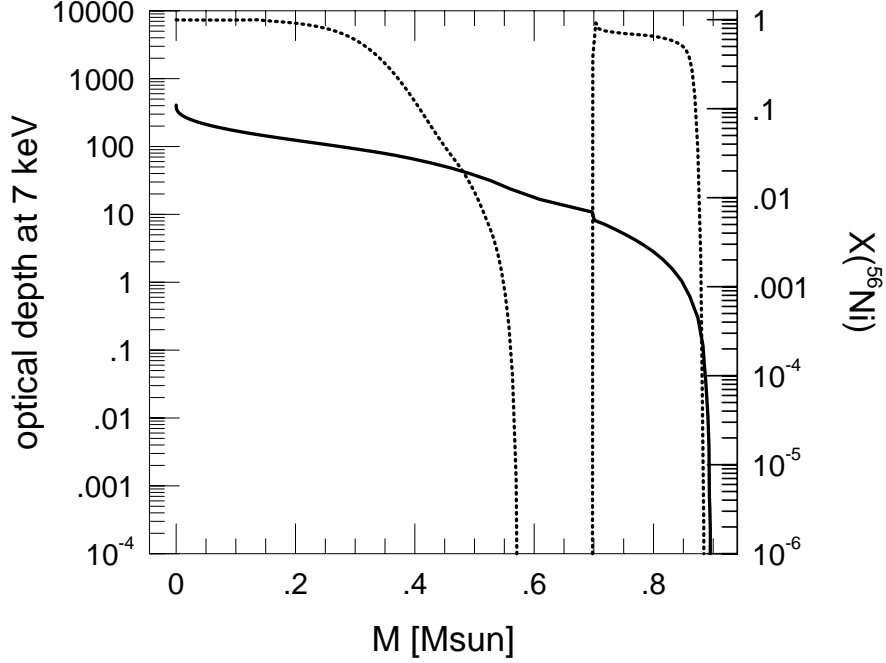


Fig. 5.— This figure shows the optical depth at 7 keV (solid line) and ^{56}Ni mass fraction (dotted line), versus mass, in Model 2 at 100 days after explosion. Only the gas situated at optical depth of order unity contributes to the emergent K-shell line flux.

where l is the total path length traversed, R is the distance between point of emission and the surface. Using $R \approx Vt$ and $\rho \sim 3M/4\pi R^3$, this can be expressed as

$$\frac{\Delta E}{E} \sim 10 \left(\frac{M}{1.4M_{\odot}} \right) \left(\frac{\kappa}{0.2} \right) \left(\frac{15 \text{ days}}{t} \right)^2 \left(\frac{8 \times 10^8 \text{ cm} \cdot \text{s}^{-1}}{v} \right) \quad (3)$$

It is this Doppler shifting of photons as they diffuse out which accounts for the fact that there is $E \sim 7$ keV X-ray continuum emission in M_{ch} models. The photons are emitted at higher energy, where the K-shell bound-free optical depth is lower, and therefore they have an enhanced chance of making it to the surface and escape. Additionally, since the abundances in the outer layers of the M_{ch} models are of lower Z , the bound-free optical depth in these layers is less than in the sub- M_{ch} case; more X-ray continuum photons from the core will make it to the surface.

In the sub- M_{ch} models, the presence of a large iron peak abundance in the outer layers ensures that the optical depth from K-shell photoabsorption is very large, preventing core X-rays from emerging at the surface. The 5-8 keV X-ray continuum in this case is due only to surface ^{56}Ni . For the sub- M_{ch} models, the controlling factor is the K-shell bound-free optical depth in the surface layers. Roughly,

$$L_{5-8 \text{ keV}} \propto [S_{56}(t) (1 - \exp(-\tau_{\gamma}))] \exp(-\tau_X), \quad (4)$$

where $S_{56}(t)$ is the γ -ray emission rate ([ergs g^{-1}]), τ_{γ} is an effective optical depth for trapping γ -rays, and τ_X is the optical depth the 5-8 keV range. The term in square brackets is a decreasing

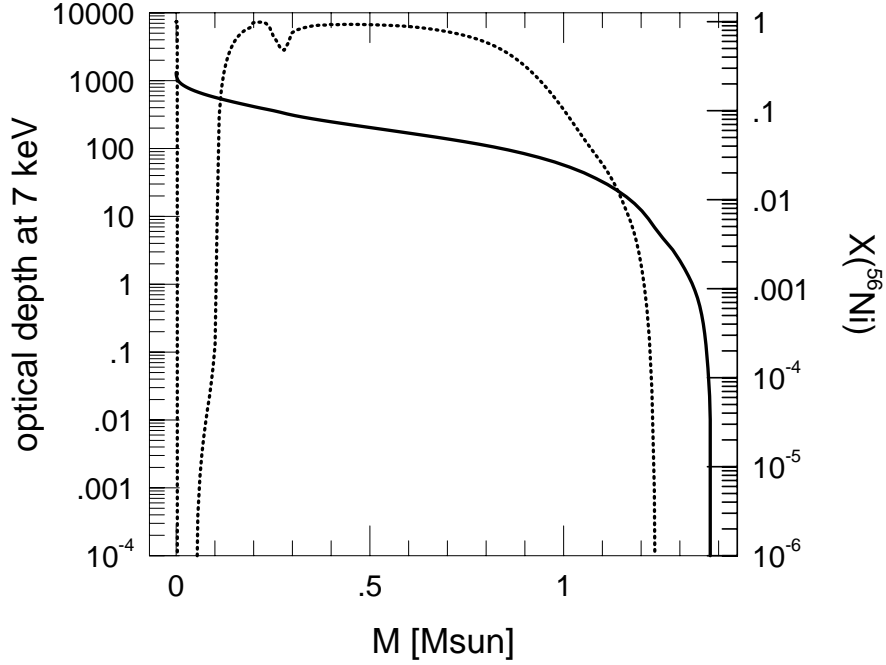


Fig. 6.— Same as Figure 5, but for Model DD4. In this case the ^{56}Ni (^{56}Co and ^{56}Fe at 100 days) sits at large optical depth, and K-shell photons produced in the core are absorbed before they are able to reach the surface.

function of time, but the $\exp(-\tau_X)$ is an increasing function of time and dominates the light curve. Thus, for the sub- M_{ch} models, the flux increases with time because more of the surface ^{56}Ni is “exposed” by the declining absorptive optical depth. For the M_{ch} models, we can write

$$L_{5-8 \text{ keV}} \propto [S_{56}(t) (1 - \exp(-\tau_\gamma))] \exp(-\tau_{X'}) \int_{\bar{E}}^{\infty} \phi(E') dE', \quad (5)$$

where $\tau_{X'}$ is the Compton optical depth at X-ray energy, in the absence of photoabsorption, $\phi(E)$ is a normalized X-ray emission distribution function, and

$$\bar{E} \sim E \left(1 + \frac{3R^2 \rho \kappa}{ct}\right). \quad (6)$$

Equation (5) expresses (very approximately) the fact that the surface flux at energy E results from emission at higher energy in the interior. At the earliest times, when the Compton optical depth is high, the Doppler shift incurred by a photon as it random walks its way out is substantial, and a large fraction of the X-rays are absorbed before arriving at the surface. As the optical depth drops, there is less Doppler shift and less absorption, and more of the X-rays can escape. Once again, the time derivative of the square bracketed term in Equation (5) is negative, while that of the second term is positive.

It is possible that vigorous hydrodynamic mixing in a M_{ch} explosion could bring enough ^{56}Ni up to the surface that the X- and γ -ray light curve would more closely resemble that of a sub-

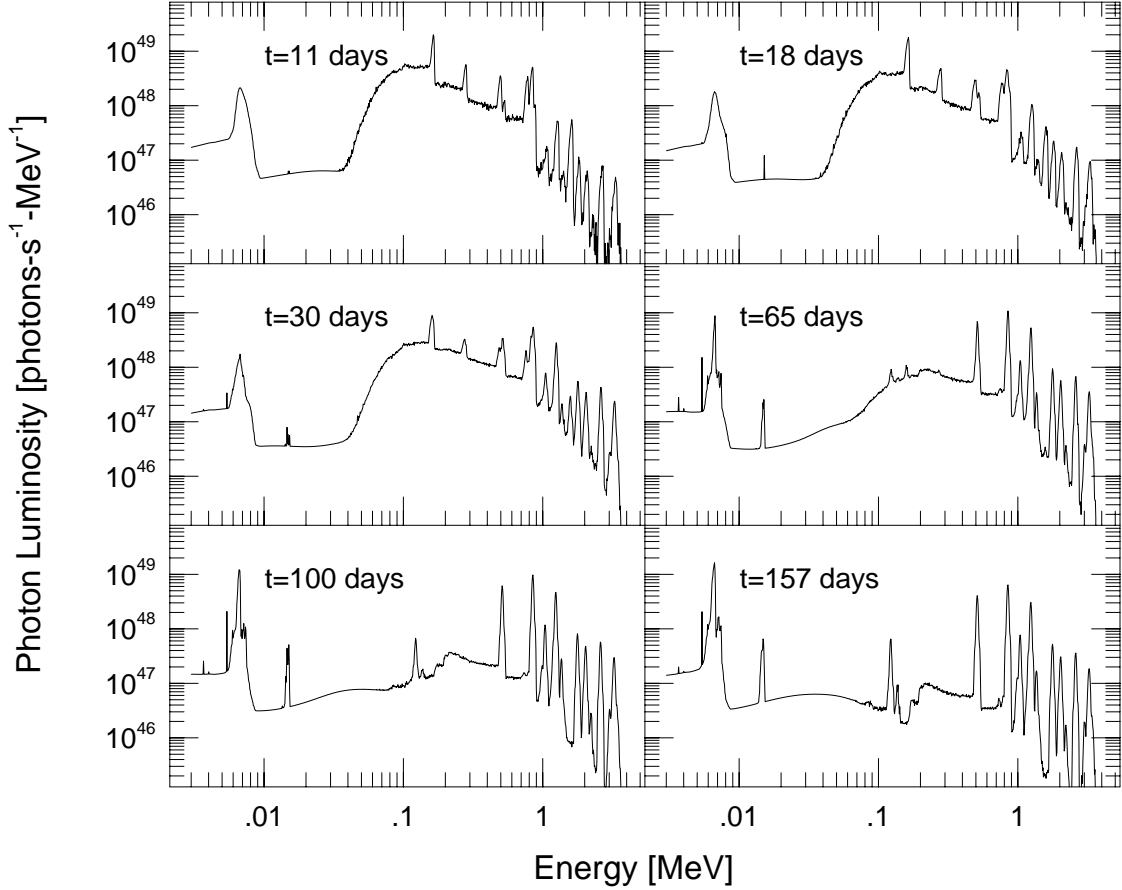


Fig. 7.— Spectral evolution of Model 2.

M_{ch} explosion than a M_{ch} explosion. As mentioned in the introduction, we regard such extensive mixing as unlikely because the compositional stratification deduced from early-time spectra would be destroyed. However, for the sake of argument, we consider the most extreme case possible, which is complete homogenization of the composition of Model DD4. This is shown in Figure 9 as Model MDD4. Unlike either the unmixed M_{ch} models or the sub- M_{ch} models, the 5 to 8 keV light curve in this case is nearly flat, and comparable in brightness, at 200 days, to the faintest of the sub- M_{ch} models considered, Model M1. The constancy of the light curve is evidently due to the deposition term in eqn (4) decreasing at the same rate that the exponential attenuation term is increasing.

Below, we discuss prospects for observing the X-ray emission from SN Ia with current, upcoming, and proposed X-ray observatories. In the case of the Chandra Observatory, the sensitivity begins to fall off dramatically beyond 5 keV and at 7 keV is quite small (effective aperture $\sim 100 \text{ cm}^2$). This precludes direct observation of iron peak K-shell emission from all but very

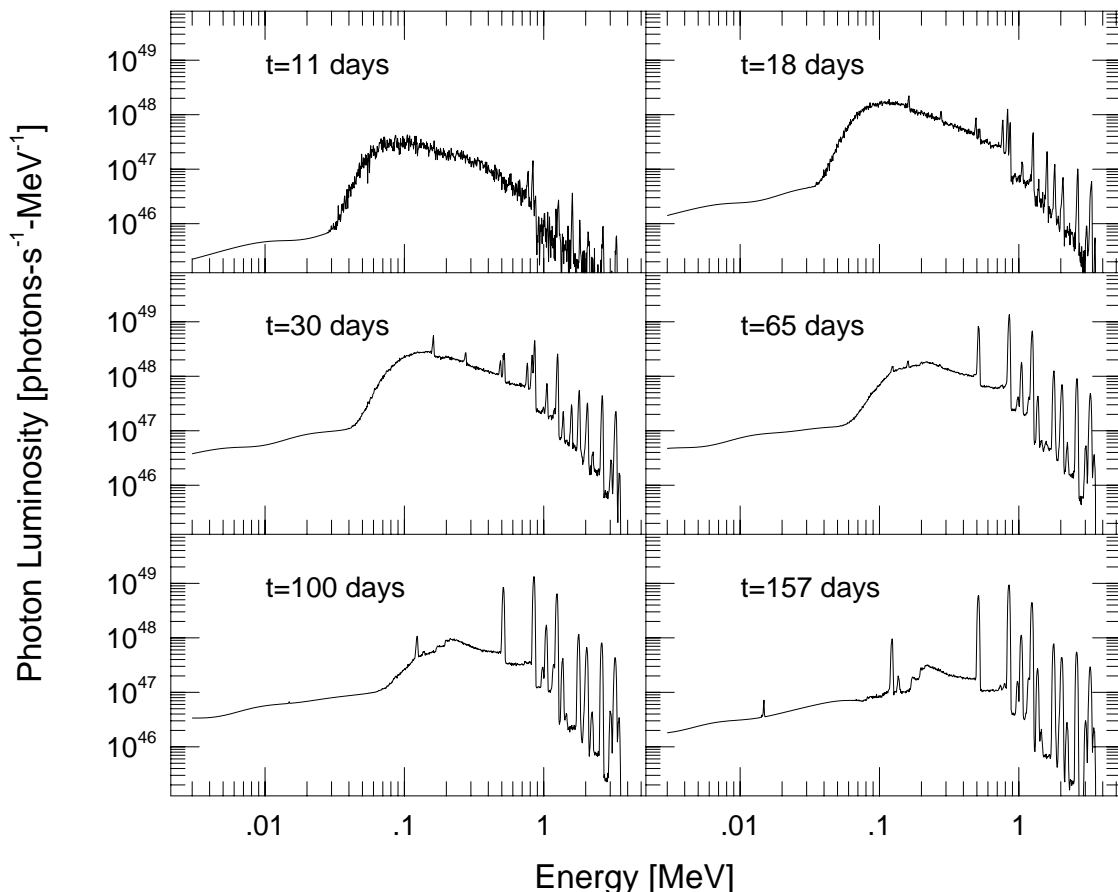


Fig. 8.— Spectral evolution of Model DD4.

nearby SNe Ia. We consider the possibility of observing a SN Ia at lower energy with Chandra; Figure 11 shows the 1-5 keV luminosity evolution for each of the models. Here we find that the faintest of the sub- M_{ch} models, Model M1, is indistinguishable from the two M_{ch} models during the first 150 days. However, from 150 days onward, the light curve flattens out and remains nearly constant for several hundred days after explosion, whereas for the M_{ch} models it drops off, with an e-folding time of ~ 130 days. Of course, model M1 would be very faint optically as well.

Most previous work on the γ -ray evolution of SNe Ia focused on the evolution of M_{ch} models (Gehrels et al. 1987; Burrows & The 1990), and especially on the ^{56}Co line evolution, since these have the greatest chance of detection from an M_{ch} SNe Ia. However, in the sub- M_{ch} models the predicted ^{56}Ni line fluxes are as much as 10 times brighter than for models such as W7 and DD4, within a factor of two as bright as their ^{56}Co lines. The ^{56}Ni 158 keV light curve for all models is shown in Figure 12. Once again, because the Compton optical depth to core ^{56}Ni remains high

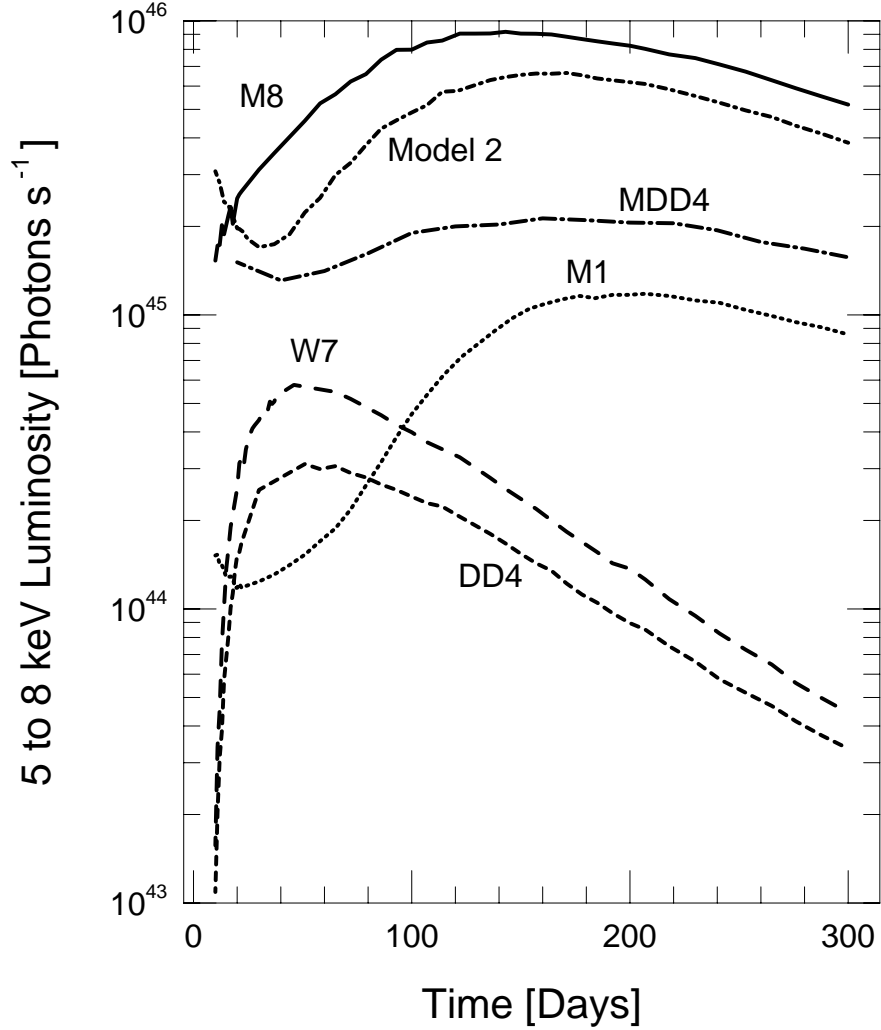


Fig. 9.— Evolution of the integrated K-shell line luminosity ($K\alpha_2$, $K\alpha_1$, $K\beta_3$, $K\beta_1$).

during the first few ^{56}Ni half-lives, the emergent flux in the sub- M_{ch} models is dominated by decay of surface ^{56}Ni . Not only are the sub- M_{ch} models brighter, but they also peak substantially earlier (~ 10 days) than the M_{ch} models (~ 30 days). Similar results are obtained for all the other ^{56}Ni decay lines. Figures 13 and 14 show the light curves for the ^{56}Ni 750 keV and 812 keV lines, respectively.

Höflich et al. (1998) have also shown that ^{56}Ni γ -ray lines peak earlier and are brighter in sub- M_{ch} explosions. Indeed, it appears from their Figure 8 that in the two sub- M_{ch} models they studied the ^{56}Ni lines reach maximum luminosity at time $t = 0$. It is not clear how this can be so. In the models studied in this paper, the exploded accretion layer has sufficient Compton optical depth to delay the maximum to ~ 10 days. Höflich et al. (1998) also predict a substantially higher luminosity in ^{56}Ni lines. For instance, their Model HeD6 is halfway between Model 2 and Model M8

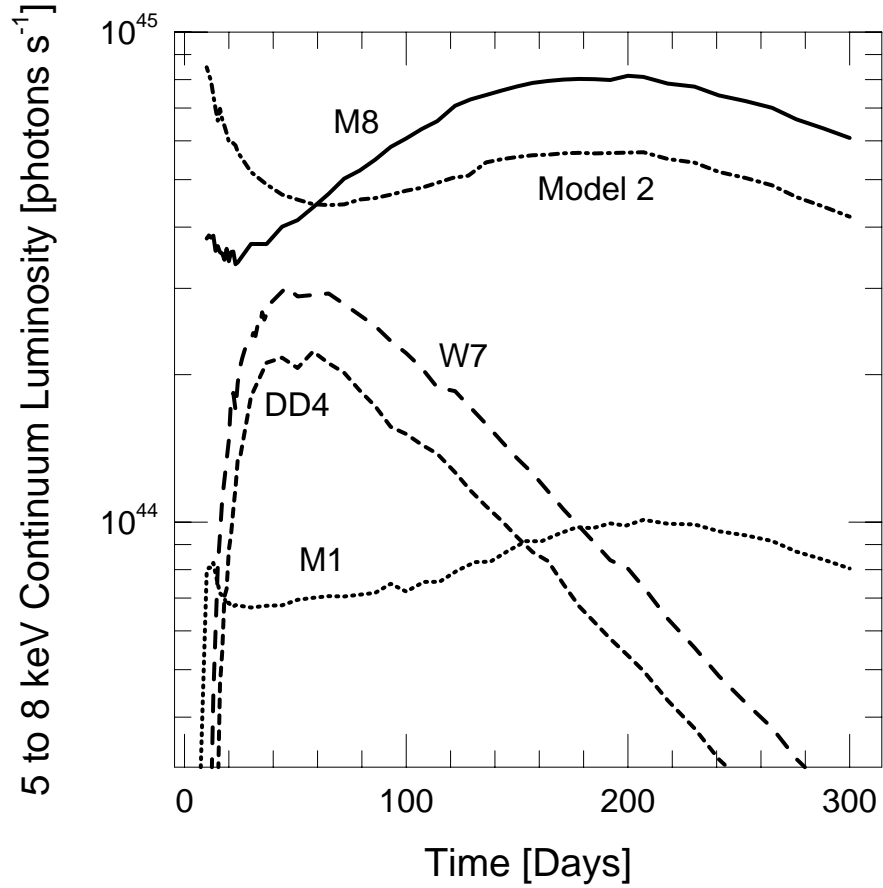


Fig. 10.— Luminosity evolution in the 5 to 8 keV bremsstrahlung continuum, excluding contributions from K-shell line emission.

in its initial mass but has nearly the same amount of surface ^{56}Ni ($0.08 M_{\odot}$) as Model 2 ($0.09 M_{\odot}$). For the ^{56}Ni 812 keV line they predict a maximum luminosity of $\sim 8.5 \times 10^{47}$ photons s^{-1} . But for Model M8, which has $0.17 M_{\odot}$ of ^{56}Ni on the surface, we obtain only $\sim 3 \times 10^{47}$ photons s^{-1} at maximum, 10 days after explosion. We cannot explain this discrepancy; to achieve their line fluxes, the surface layers must expand with a much higher velocity than in Models 2, M1, or M8. We note that our line transport results have been verified by performing the calculations by both Monte Carlo and deterministic methods, as described in the last section; consistent results were obtained between the two methods in all cases.

The situation is quite different for ^{56}Co lines. The light curves for ^{56}Co 847 keV and 1238 keV are shown in Figures 15 and 16, respectively. Since ^{56}Co is so much longer-lived than ^{56}Ni ($t_{1/2} = 77.1$ days versus 6.1 days), the light curves for these lines reach maximum once the Compton optical depth to the core is less than 1, which happens at around 50 days past explosion. The M_{ch} and sub- M_{ch} models are distinguishable by the rise time, which is earlier in the sub- M_{ch} models, but this might be difficult to detect, particularly for objects which are only marginally within

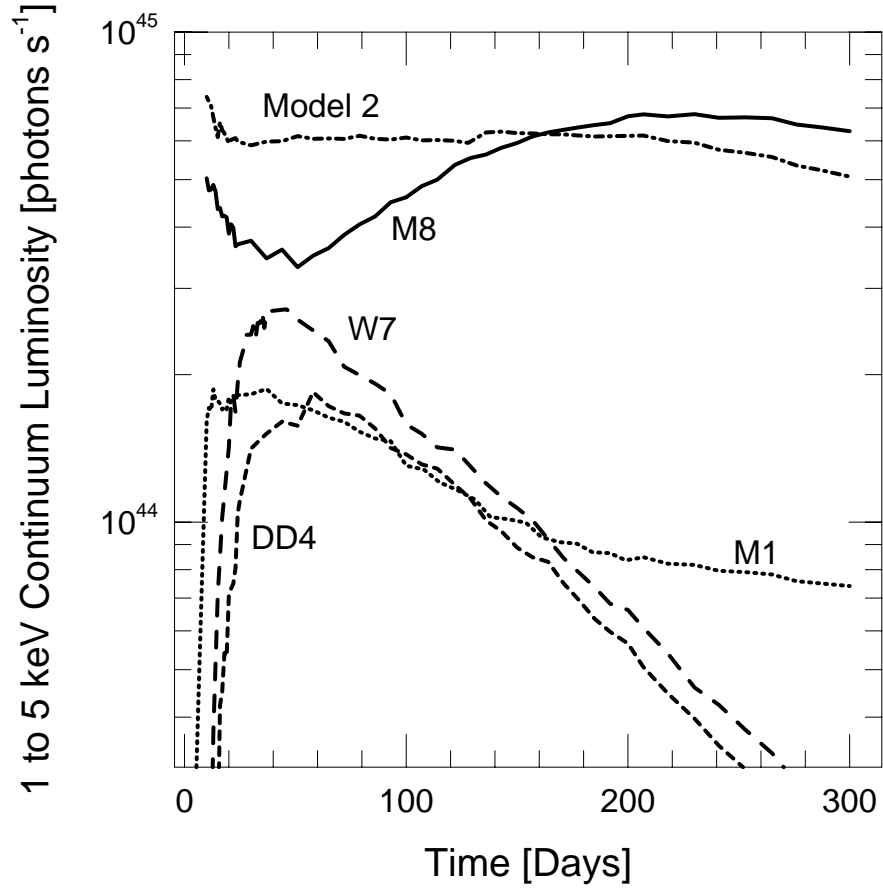


Fig. 11.— Luminosity evolution in the 1 to 5 keV continuum.

detection limits at maximum brightness. Differences in the core ^{56}Ni mass can mask the effect of any contribution from surface ^{56}Ni .

4. Prospects for Detection

Measurement of the 7 keV K-shell emission from Type Ia supernovae provides a direct and straightforward basis for discriminating between the two current classes of progenitor models. Detection of a large K-shell line flux or bright bremsstrahlung continuum would indicate surface ^{56}Ni , which at present is predicted in significant quantities only from the sub- M_{ch} model for Type Ia supernovae. Additionally, the light curves of ^{56}Ni γ -ray decay lines from sub- M_{ch} models are distinctly different than for M_{ch} models, providing an unambiguous indication of the presence or absence of ^{56}Ni at the surface.

Unfortunately, prospects are at best marginal for detecting X-ray emission from a SN Ia at a distance as great as Virgo using the current generation of X-ray observatories. XMM, which was

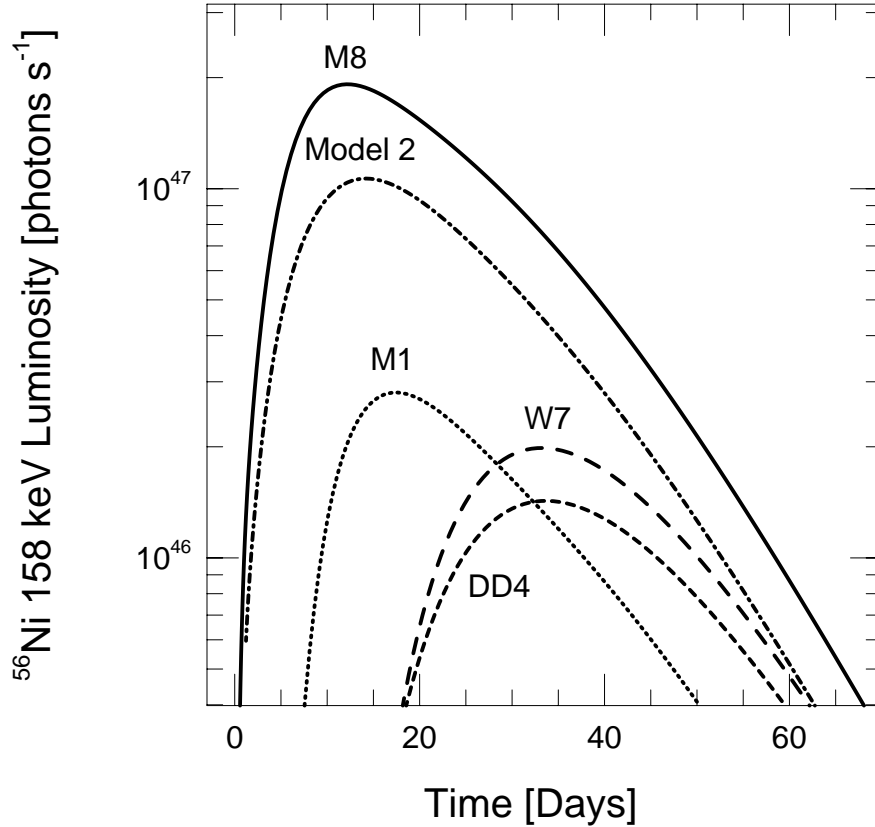


Fig. 12.— The ^{56}Ni 158 keV light curve for all models. The sub- M_{ch} models are up to ~ 10 times brighter, and peak substantially earlier (~ 10 days) than the M_{ch} models (~ 30 days).

launched 10 December 1999, has the largest effective aperture at 7 keV of current and near-term missions. We have used the XMM simulator (SCISIM) to assess the likelihood of detection for the X-ray spectrum of Model 2 at 100 days. Assuming a nominal distance of 15 Mpc, the integrated 5-10 keV flux is 1.82×10^{-7} photons $\text{s}^{-1} \text{cm}^{-2}$. Using both EPIC MOS CCDs and the PN CCD, and assuming a half-power diameter of $15''$, 10 counts would be detected in a 10^5 second exposure. Although this may seem like a small number, XMM’s background count rate in the 5-10 keV range is very low, ($\approx 1.7 \times 10^{-5}$ counts s^{-1}); the estimated background is 1.7 counts, making this (formally) a 7σ detection. Although this will not provide the type of detailed kinematic information which, ideally, one would like to have to confirm the origin of the counts, it is nonetheless sufficient to distinguish with high confidence between the M_{ch} and sub- M_{ch} models for Type Ia supernovae.

The prospects for detecting a sub- M_{ch} SNe Ia with the Chandra X-ray Observatory are lower: at 7 keV the effective aperture of Chandra is roughly 100 cm^2 for the ACIS-S imaging spectrometer; under the previous assumptions this would give only 2 photons in a 10^5 second exposure. The sensitivity is higher at lower energy, but the supernova is also fainter. The total photon flux from Model M8 at 15 Mpc is 3.4×10^{-9} photons s^{-1} in $1\text{keV} < E < 2\text{keV}$, and 1.5×10^{-8}

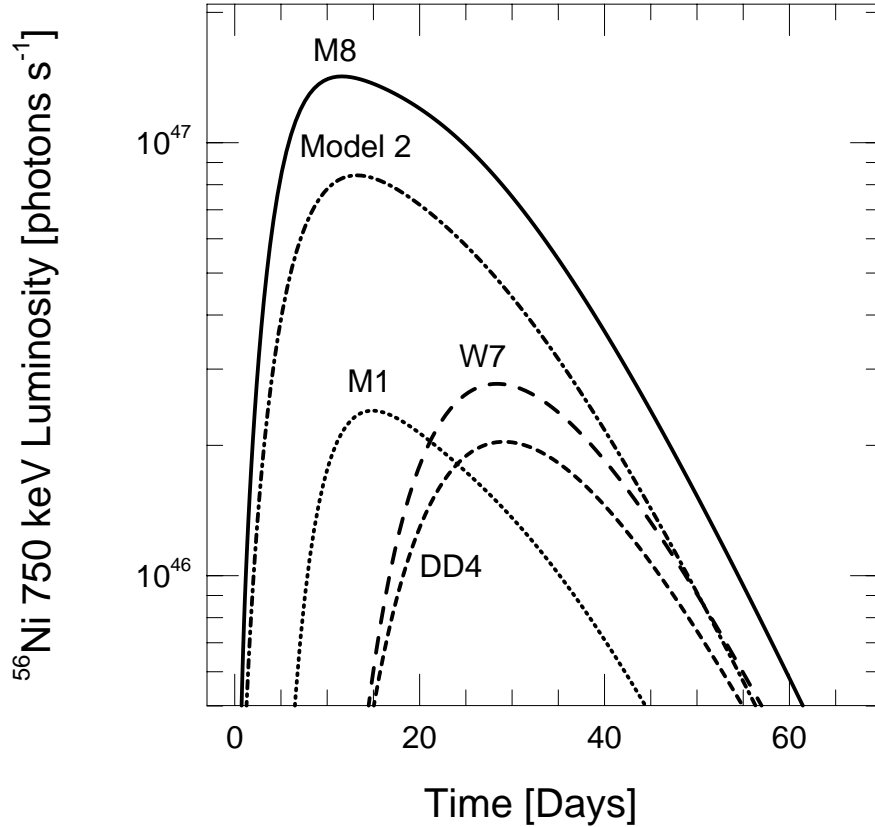


Fig. 13.— Same as Figure 12, but for the ^{56}Ni 750 keV line.

photons s^{-1} in $2\text{keV} < E < 5\text{keV}$. The effective aperture of the ASCA Imaging Spectrometer in the $1\text{keV} < E < 2\text{keV}$ range is approximately 600 cm^2 . Consequently, a 10^6 second observation would result in only 2 counts. For the $2\text{keV} < E < 5\text{keV}$ range, the effective aperture is approximately 300 cm^2 and the number of counts is approximately 4.5. Both of these count rates would be lost in the noise, which is substantially greater.

The proposed Constellation-X Observatory (Con-X: see <http://constellation.gsfc.nasa.gov>) offers the best hope for high resolution spectroscopy of K-shell emission from a sub- M_{ch} SNe Ia in Virgo. The proposal calls for Con-X's effective area to be $15,000\text{ cm}^2$ at 1 keV , and $6,000\text{ cm}^2$ at 6.4 keV . Using the assumptions above, the number of counts received in 10^5 seconds would be 110 photons. Con-X might also be able to detect the lower energy bremsstrahlung continuum. In Model 2 at 100 days, the integrated 1-5 keV continuum flux at 15 Mpc would be $2 \times 10^{-8}\text{ s}^{-1}$. Taking the mean aperture over this energy range to be $11,000\text{ cm}^2$, the number of counts in a 10^5 second exposure is 21 photons.

Immediate prospects for detecting ^{56}Ni γ -line emission are less promising. As an example, the peak 812 keV luminosity for model M8 is $\sim 2 \times 10^{47}$ photons s^{-1} (Figure 14). At 15 Mpc this corresponds to a flux of 7.4×10^{-6} photons $\text{cm}^2\text{ s}^{-1}$, which is just *at* the sensitivity limit for

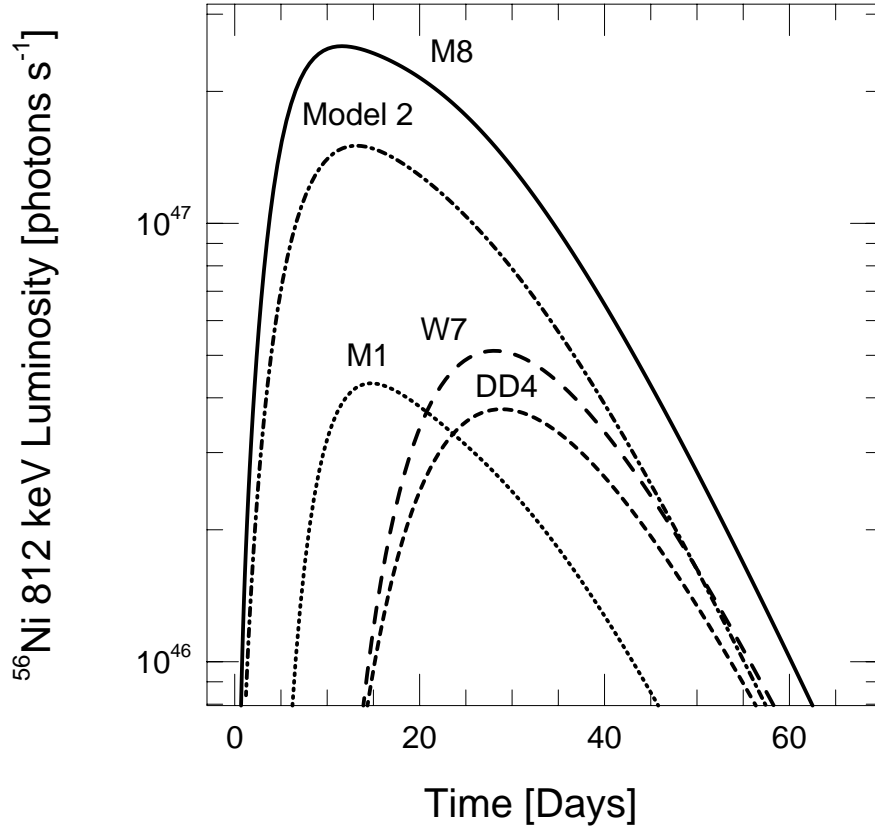


Fig. 14.— Same as Figure 12, but for the ^{56}Ni 812 keV line.

INTEGRAL to detect narrow lines in a 10^6 second observation (Winkler 1998). As Timmes & Woosley (1997) have pointed out, flux levels such as produced by the present set of sub- M_{ch} models could easily be seen with the proposed ATHENA γ -ray Observatory (Johnson et al. 1995).

The view of Höflich et al. (1998) for detecting ^{56}Ni in sub- M_{ch} explosions with INTEGRAL was slightly more optimistic than ours. However, as described in the proceeding section, their predicted line luminosities are much higher than ours, peaking almost immediately after explosion.

5. γ -Line Profiles

While neither current nor planned γ -ray spectroscopy missions are sufficiently sensitive to obtain useful profile data from other than a *very* nearby supernova, line profiles may some day serve as another possible probe of the radial distribution of radioactivity.

Figure (17) shows the evolution of the ^{56}Ni 1.562 MeV and ^{56}Co 1.772 MeV line profiles. While these are weak lines, they are representative, and their proximity in energy makes them a good illustration of the difference in evolution of the ^{56}Ni and ^{56}Co emission. Because Compton

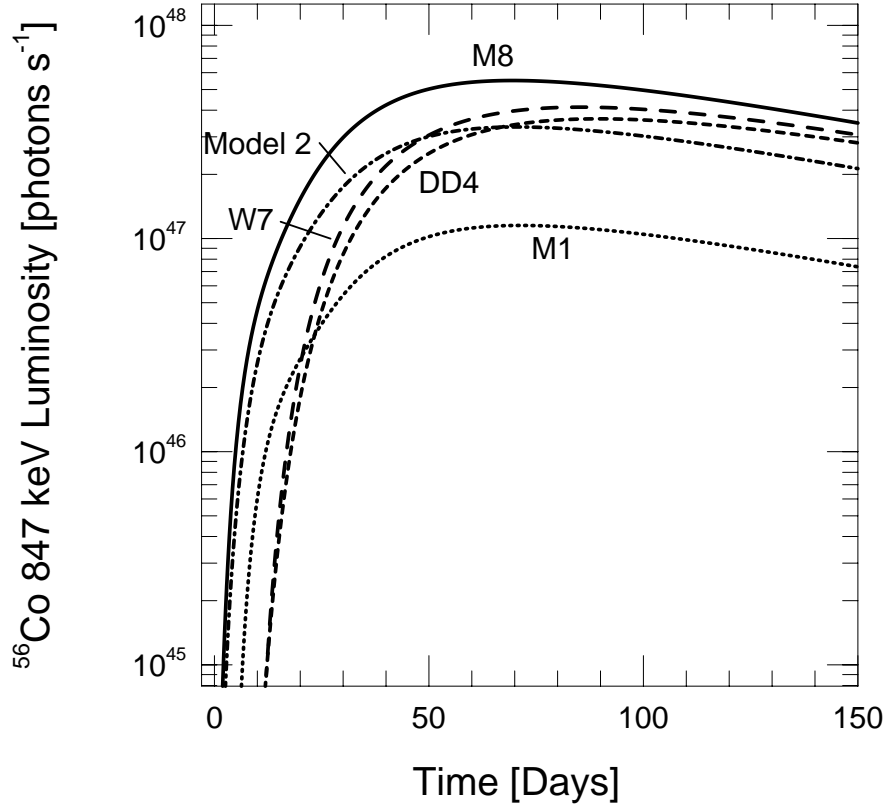


Fig. 15.— The ^{56}Co 847 keV light curve for all models. Although the sub- M_{ch} light curve rises more quickly than does the M_{ch} light curves, the differences in maximum brightness depend only on the total mass of ^{56}Ni produced.

scattering through any appreciable angle removes photons from the profile altogether, the line shapes reflect the velocity distribution of radioactive material at low optical depth to the observer.

In the M_{ch} models, radioactive material is only found deep within the supernova. Initially (15 days), the radiation which escapes is from material closest to the observer (γ -rays emitted from material on the far side, away from the observer, see too large an optical depth, and are absorbed). The peak intensity of the line is therefore blue-shifted by $\sim 6000\text{km s}^{-1}$, and the line is very weak as a consequence of the large optical depth. There is also a broad wing to the red resulting from Compton scattering. As the ejecta expand and the column depth decreases, a larger volume of the ejecta become visible and the red side of the profile increases in intensity. By 100 days, the ejecta are nearly transparent (optical depth to the center at 1 MeV is unity) and the profile is that of an expanding optically thin sphere, symmetric about the rest energy of the line. This is clearly seen in the ^{56}Co profile, which reaches its maximum intensity at about this time. The short half-life of ^{56}Ni ensures that by the time the profile has shifted back to the rest energy it has disappeared.

In the sub- M_{ch} models, the high velocity ^{56}Ni layer on the outside leads to ^{56}Ni and ^{56}Co

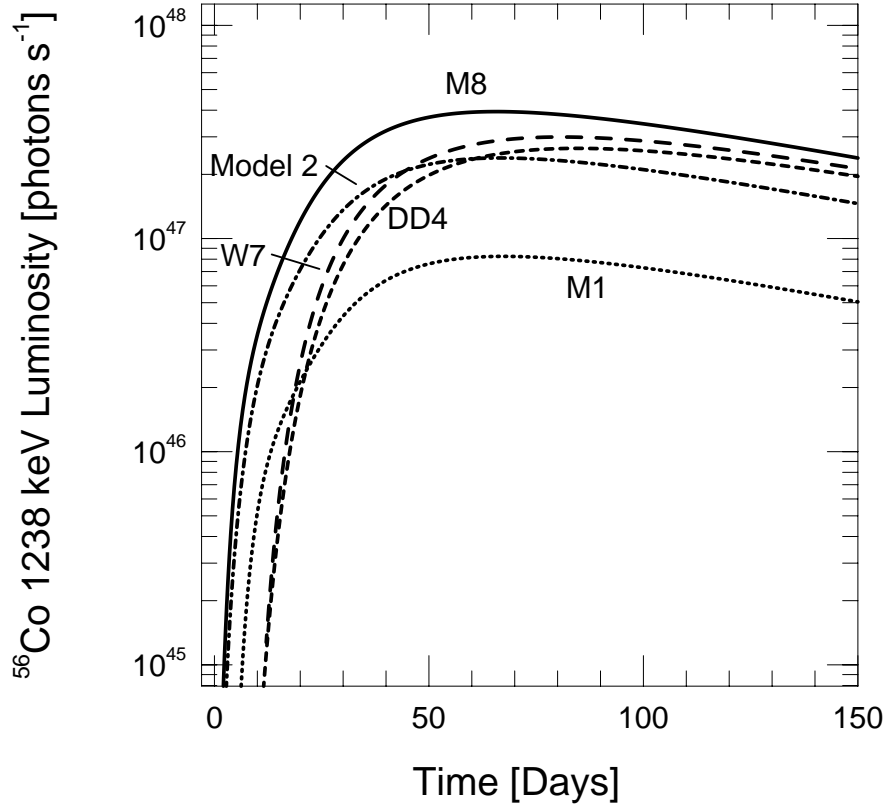


Fig. 16.— Same as Figure 15, but for the ^{56}Co 1238 keV line.

lines with rapid rise times (*c.f.* Figures 12 and 15). At the earliest times (15 days), the only optically-thin paths are those from the side approaching the observer. The resulting line centers are blue-shifted by 7000 km s^{-1} with wings extending up to $20,000 \text{ km s}^{-1}$ to the blue. As the ejecta expand (25 days), the optical depth through to surface layers expanding on the opposite side of the supernovae becomes smaller, and the red wings of the profiles increase in intensity. While the core radioactivity is becoming visible, it makes only a small contribution at this time. By 50 days, however, emission from the core dominates the profile, which is now virtually identical to the M_{ch} model but for the low intensity but very broad wings from the outer layer. In this model, the ^{56}Ni lines are proportionately much stronger at early times due to the low optical depth to the surface layers; its short decay time ensures that the ^{56}Ni lines will always be observed to have higher energies than at rest.

6. Summary

In this paper we have presented results of X- and γ -ray transport calculations of M_{ch} and sub- M_{ch} explosion models for Type Ia supernovae. We have shown that the X-ray and γ -ray spectral

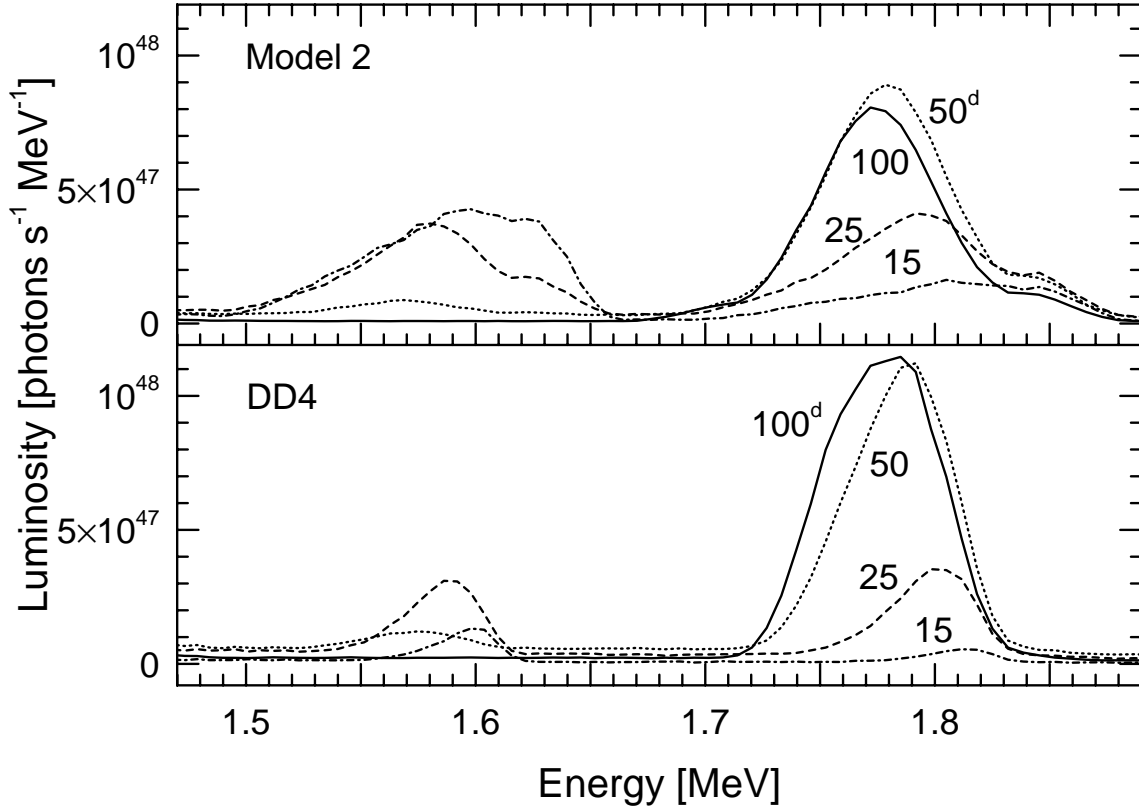


Fig. 17.— Evolution of the ^{56}Ni 1.562 MeV and ^{56}Co 1.772 MeV line profiles. The top panel shows the evolution of these lines for the sub- M_{ch} model hedtb11 at four different times; the bottom panel shows results from the M_{ch} model DD4.

evolution of sub- M_{ch} models is distinctly different than M_{ch} models. The presence of surface ^{56}Ni in sub- M_{ch} supernovae would make them extremely bright emitters of iron peak K-shell emission, visible for several hundred days after explosion. K-shell emission from a bright sub- M_{ch} located in the neighborhood of Virgo would be just above the limit for detection by the XMM Observatory. Detection by CHANDRA is unlikely for a SNe Ia as distant as Virgo.

Likewise, the ^{56}Ni γ -ray light curves all display a substantially different behavior in sub- M_{ch} and M_{ch} models. Because of the presence of ^{56}Ni on the surface, the former are much brighter and peak much earlier than in M_{ch} supernovae (~ 10 versus ~ 30 days). The ^{56}Ni γ -ray line emission from a bright sub- M_{ch} explosion at 15 Mpc would be just at the limit for detection by INTEGRAL.

Moderate resolution spectroscopy of γ -ray lines would allow studying the evolution of line

profiles. This would provide the most detailed and readily interpreted data on the distribution of radioactive elements and column density in SNe Ia. Unfortunately, there are at present no plans to construct an instrument with sufficient aperture to observe any but the very closest (and rarest) SNe Ia in such detail.

We greatly appreciate useful discussions with Dave Arnett and Stan Woosley. We are particularly grateful to Patrick Woźdowski for his invaluable assistance with the instrument simulations, and to Lynn Kissel for his assistance with the bremsstrahlung crosssections.

This work was supported by the UC Lawrence Livermore National Laboratory and the US Department of Energy (W-7405-ENG-48), and by the National Science Foundation (CAREER grant AST9501634, PAP). PAP gratefully acknowledges support from the Research Corporation though a Cottrell Scholarship. TR gratefully acknowledges the support of a graduate fellowship from the National Physical Sciences Consortium.

REFERENCES

- Arnett, W. D. 1980, *ApJ*, 157, 1369
- Axelrod, T. S. 1980, Ph.D. thesis, University of California Santa Cruz
- Brachwitz, F., et al. 2000, *ApJ*, submitted to *ApJ*
- Burrows, A., Shankar, A., & van Riper, K. A. 1991, *ApJ*, 379, L7
- Burrows, A., & The, L.-S. 1990, *ApJ*, 360, 626
- Cappellaro, E., Turatto, M., Tsvetkov, D. Y., Bartunov, O. S., Pollas, C., Evans, R., & Hamuy, M. 1997, *A&A*, 322, 431
- Clayton, D. D., Colgate, S. A., & Fishman, G. J. 1969, *ApJ*, 155, 75
- Clayton, D. D., & The, L.-S. 1991, *ApJ*, 375, 221
- Colgate, S. A., & McKee, C. 1969, *ApJ*, 157, 623
- Contardo, G., & Leibundgut, B. 1998, in *Proceedings of the 9th workshop on Nuclear Astrophysics*, 128
- Eastman, R. G. 1996, in *Thermonuclear Supernovæ*, ed. R. Canal, P. Ruiz-Lapuente, & I. J. (Kluwer:Dordrecht), 571
- Eastman, R. G., & Pinto, P. A. 1993, *ApJ*, 412, 731
- Eastman, R. G., Woosley, S. E., Weaver, T. A., & Pinto, P. A. 1994, *ApJ*, 430, 300

- Gehrels, N., Leventhal, M., & MacCallum, C. J. 1987, *ApJ*, 322, 215
- Gehrels, N., Leventhal, M., & MacCallum, C. J. 1988, in *Nuclear Spectroscopy of Astrophysical Sources*, AIP Conf Proc. No. 170, ed. N. Gehrels & G. Share (AIP: New York), 87
- Hamuy, M., & Pinto, P. A. 1999, *AJ*, 117, 1185
- Harkness, R. 1991, in *Supernovae; The Tenth Santa Cruz Summer Workshop in Astronomy and Astrophysics*, ed. S. E. Woosley (Springer-Verlag: New York), 454
- Höflich, P., Khokhlov, A. M., Wheeler, J. C., Phillips, M. M., Suntzeff, N. B., & Hamuy, M. 1996, *ApJ*, 472, L81
- Höflich, P., Müller, E., & Khokhlov, A. 1993, *Å*, 268, 570
- Höflich, P., Wheeler, J. C., & Khokhlov, A. 1998, *ApJ*, 492, 228
- Iben, J., Icko, & Tutukov, A. V. 1991, *ApJ*, 370, 615
- Iglesias, C. A., Rogers, F. J., & Wilson, B. G. 1990, *ApJ*, 360, 221
- Iglesias, C. A., Rogers, F. J., & Wilson, B. G. 1992, *Revista Mexicana de Astronomia y Astrofisica*, vol. 23, 23, 9
- Johnson, W. N., et al. 1995, *SPIE*, 2518, 74
- Kaastra, J. S., & Mewe, R. 1993, *A&AS*, 97, 443
- Khokhlov, A. M., Oran, E. S., & Wheeler, J. C. 1997, *ApJ*, 478, 678
- Kirshner, R. P., et al. 1993, *ApJ*, 415, 589
- Kissel, L., Crawford, M., & Pratt, R. H. 1991, Bremsstrahlung energy spectra from electrons of kinetic energy $1 \text{ keV} \lesssim 2000 \text{ keV}$ incident on neutral atoms $1 \lesssim z \lesssim 92$, Technical Report SAND81-1337, Sandia National Laboratory
- Kuchner, M. J., Kirshner, R. P., Pinto, P. A., & Leibundgut, B. 1994, *ApJ*, 426, L89
- Kurucz, R. L. 1991, in *Stellar Atmospheres: Beyond Classical Models*, ed. L. Crivellari, I. Hubeny, & D. G. Hummer (Kluwer:Dordrecht), 441
- Limongi, M., & Tornambe, A. 1991, *ApJ*, 371, 317
- Livne, E. 1990, *ApJ*, 354, L53
- Livne, E., & Arnett, D. 1995, *ApJ*, 452, 62
- Livne, E., & Glasner, A. S. 1991, *ApJ*, 370, 272

- Niemeyer, J. C., & Woosley, S. E. 1997, *ApJ*, 475, 740
- Nomoto, K., Thielemann, F. K., & Yokoi, K. 1984, *ApJ*, 286, 644
- Nugent, P., Baron, E., Branch, D., Fisher, A., & Hauschildt, P. H. 1997, *ApJ*, 485, 812
- Phillips, M. M. 1993, *BAAS*, 182, 2907
- Pinto, P. A. 1997, in *Thermonuclear Supernovæ*, ed. R. Canal, P. Ruiz-Lapuente, & I. J. (Kluwer:Dordrecht), 607
- Pinto, P. A., & Eastman, R. G. 2000a, *ApJ*, in press
- Pinto, P. A., & Eastman, R. G. 2000b, *ApJ*, in press
- Pinto, P. A., & Woosley, S. E. 1987, *BAAS*, 19, 1050
- Pinto, P. A., & Woosley, S. E. 1988a, *Nature*, 333, 534
- Pinto, P. A., & Woosley, S. E. 1988b, *ApJ*, 329, 820
- Pinto, P. A., Woosley, S. E., & Ensman, L. M. 1988, *ApJ*, 331, L101
- Riess, A. G., et al. 1999, *ApJ*, submitted
- The, L.-S., Bridgman, W. T., & Clayton, D. D. 1994, *ApJS*, 93, 531
- Timmes, F. X., & Woosley, S. E. 1997, *ApJ*, 489, 160
- Timmes, F. X., Woosley, S. E., & Weaver, T. A. 1995, *ApJS*, 98, 617
- van den Bergh, S., & Tammann, G. A. 1991, *ARA&A*, 29, 363
- Weaver, T. A., Axelrod, T., & Woosley, S. E. 1980, in *Type Ia Supernovæ: Proceedings of the Texas Workshop*, Austin, TX, March 17-19, 1980, ed. J. Wheeler (University of Texas at Austin ; [Fort Davis, Tex.]), 113
- Winkler, C. 1998, in *Proceedings 3rd INTEGRAL Workshop*, Taormina 1998
- Woosley, S. E., & Weaver, T. A. 1986, *ARA&A*, 24, 205
- Woosley, S. E., & Weaver, T. A. 1991, in *Les Houches, Session LIV*, ed. J. Audouze, S. Bludman, R. Mochkovitch, & J. Zinn-Justin (Elsevier Science Publishers)
- Woosley, S. E., & Weaver, T. A. 1994, *ApJ*, 423, 371
- Xu, Y. 1989, Ph.D. thesis, University of Colorado, Boulder
- Xu, Y., Ross, R. R., & McCray, R. 1991, *ApJ*, 371, 280

Table 2: K-shell Lines

transition	E [keV]	yield
Fe $K\alpha_2$	6.3915	0.1013
Fe $K\alpha_1$	6.4047	0.2026
Fe $K\beta_3$	7.0567	0.0127
Fe $K\beta_1$	7.0583	0.0254
Co $K\alpha_2$	6.9151	0.1084
Co $K\alpha_1$	6.9295	0.2168
Co $K\beta_3$	7.6472	0.0136
Co $K\beta_1$	7.6489	0.0272
Ni $K\alpha_2$	7.4611	0.1226
Ni $K\alpha_1$	7.4782	0.2451
Ni $K\beta_3$	8.2623	0.0154
Ni $K\beta_1$	8.2642	0.0309

Table 2: Fe, Co and Ni K-shell lines produced by sub- M_{ch} SNe Ia (taken from Kaastra & Mewe 1993).